JJ

GSI

GSI-Preprint-97- 42
August 1997

MOMENTUM SPECTRA FOR SINGLE AND DOUBLE ELECTRON IONIZATION OF He IN RELATIVISTIC COLLISIONS

C. J. Wood, R. E.,Olson, W. Schmitt, R. Moshammer, J. Ullrich

(Submitted to Phys. Rev. A)

Gesellschaft für Schwerionenforschung mbH
Planckstraße 1 • D-64291 Darmstadt • Germany
Postfach 11 05 52 • D-64220 Darmstadt • Germany

Momentum Spectra for Single and Double Electron Ionization of He in Relativistic Collisions

C. J. Wood*, R. E. Olson*, W. Schmitt#, R. Moshammer#, and J. Ullrich#

*Department of Physics, University of Missouri-Rolla, Rolla, MO 65401, USA

#Gesellschaft für Schwerionenforschung, Planckstraße 1, D-64291 Darmstadt, Germany

Abstract

The complete momentum spectra for single and double ionization of He by 1 GeV/u ($\beta = 0.88$) U^{92+} have been investigated using a classical trajectory Monte Carlo method corrected for the relativistic projectile. The $1/r_{12}$ electron-electron interaction has been included in the post-collision region for double ionization to incorporate the effects of both the nuclear-electron and electron-electron ionizing interactions, and to access the effects of electron correlation in the electron spectra. Experimental measurements were able to determine the longitudinal momentum spectra for single ionization; these observations are in accordance with the theoretical predictions for the three-body momentum balance between projectile, recoil ion, and ionized electron. In particular, the Lorentz contraction of the coulomb interaction of the projectile manifests itself in the decrease of the post-collision interaction of the projectile with the electron and recoil ion, causing them to recoil back-to-back as in the case for a short electromagnetic pulse. This feature is clearly displayed in both the theoretical and experimental longitudinal momentum spectra, and by comparing to calculations that are performed at the same collision speed but do not include the relativistic potentials. Moreover, collision plane spectra of the three particles demonstrate that the momenta of the recoil ion and ionized electron are preferentially equal, and opposite, to each other. The electron spectra for double ionization show that the inclusion of the electron-electron interaction in the post-collision regime partitions the combined ionization momentum of the electrons so that the electrons are preferentially emitted in opposite azimuthal angles to one another. This is in contrast to calculations made assuming independent electrons.

PACS: 34.50.Fa, 34.10.+x

Introduction

The development and combination of the fields of recoil ion and electron momentum spectroscopy now allows one to perform complete momentum experiments of all reaction products for single and double ionization collisions: e.g. see reviews by Ullrich *et al.*[1], Cocke and Olson[2], and recent experiments by Moshammer *et al.*[3-5]. Concurrent with these experimental developments, the standard three-body classical trajectory Monte Carlo (CTMC) method[6,7] has been refined to describe recoil ion spectra for multiple electron removal processes, including the differential emission of multiply-ionized electrons[8,9]. Most recently, a CTMC model for He that employs Hartree Fock screening potentials has been developed which dynamically varies the screening parameters during the collision in order to more realistically describe double ionization[10,11]. This model has been extended to include the $1/r_{12}$ electron-electron interaction in the post-collision region and has been successful in describing the correlation of the emitted electrons in 3.6 MeV/u Se^{28+} + He double ionization collisions[4]. Since the $1/r_{12}$ electron-electron interaction is incorporated in the collision at the time when the energy of the first electron becomes positive, the method inherently includes the electron-electron induced double ionization process along with the projectile-electron interactions. The inclusion of the $1/r_{12}$ interaction in the post-collision regime is critical to the understanding of transfer ionization dynamics[12] and the correct evolution of the effective projectile charge seen by the residual target. The latter characteristic manifests itself in a decrease of post-collision interaction with the projectile which is necessary to understand longitudinal momentum spectra for multiple electron removal by low charge state ions[13].

At present, the CTMC method is the only theoretical method available which provides complete momenta information for single and multiple electron ionization collisions. This feature allows one to investigate the detailed dynamics of electron removal in terms of the momentum balance between all products in 3- or n-body collisions. Moreover, collision plane studies of the momentum spectra provide a detailed probe of the various mechanisms responsible for electron removal in proton, anti-proton, and multiply-charged ion collisions[14,15].

For the system under study in this paper, 1 GeV/u U^{92+} + He, the theoretical method employed by Moshammer *et al.*[4] has been further extended to include the relativistic interaction

of the projectile on the He target. This ensures a full four-body calculation, including the electron-electron interaction in the post collision region for double ionization. Although the collision is relativistic with $\beta = v/c = 0.88$, the charge of the fully-stripped U^{92+} increases the perturbation strength of projectile charge divided by collision speed to $q/v = 0.76$. Thus, the collision is not in the low q/v perturbation regime, but where the CTMC method shows applicability[16].

It is the goal of this paper to utilize the four-body CTMC method to present kinematically complete momentum spectra that can help in the understanding of relativistic collision dynamics[17]. Our calculations involve all the particles in the collision, and as such, complement those made assuming the Weizsäcker-Williams equivalent photon method[18,19]. With this latter method, Keller *et al.*[20] have explored the effects of electron correlation on the double ionization spectra of He. They conclude from calculations made for a fixed impact parameter of 5 a_o, that both initial state and post-collision electron-electron interactions are required to fully describe the ejected electron data.

Theoretical Method

The aim of this theoretical work is to incorporate effects of a bare, highly charged projectile impacting on a light target atom at a relativistic velocity into the Classical Trajectory Monte Carlo (CTMC) method. The CTMC method has been successful in predicting total ionization and capture cross sections at non-relativistic impact velocities, and also cross sections differential in various final state energies and momenta. More recent applications of this method display the ability to completely describe the final state kinematics of various ionization reactions. This has been achieved by using the dynamic dCTMC method[10,11], which incorporates dynamical screening to describe the He target.

In order to correctly describe a two electron process such as double or transfer ionization, the electron-electron interaction must be included in the theoretical model. By using the dCTMC method, electron-electron interactions in the He ground state are approximated by applying Hartree-Fock model potentials with dynamically varying screening parameters which depend on the collision conditions. However, if both electrons are ejected from the atom, the screening of the model potential is zero, therefore no final state correlation between the electrons is available. This will result in incorrect momentum distributions for all products. In order to achieve the desired post collision correlation, the Coulomb interaction between the electrons is employed after the first electron is ejected from the He atom. The interaction is exponentially increased in collision time until the full $1/r_{12}$ is included, which ensures the correct asymptotic boundary conditions for all particles in the final state. This procedure, termed the rCTMC method, has been successful in the treatment of double ionization of helium by Se^{28+} at 3.6 MeV/u , where electron correlation was exhibited in electron longitudinal momentum distributions[4]. Moreover, since the $1/r_{12}$ interaction is dynamically incorporated during the collision, both the electron-nuclear and electron-electron interactions are included for double electron removal reactions. This aspect was critical to understanding the electron-electron Thomas scattering observed by Mergel *et al.* for the H^+ + He transfer ionization process[12]. As in these publications, the complete kinematic information will be calculated for the final momentum states of the reaction products.

In an exact relativistic treatment, the electric and magnetic fields

$$\boldsymbol{E}=[\frac{\boldsymbol{n}-\boldsymbol{\beta}}{\gamma^2(1-\boldsymbol{\beta}\cdot\boldsymbol{n})^3R^2}]_{ret}+\frac{1}{c}[\frac{\boldsymbol{n}\times\{(\boldsymbol{n}-\boldsymbol{\beta})\times\dot{\boldsymbol{\beta}}\}}{(1-\boldsymbol{\beta}\cdot\boldsymbol{n})^3R}]_{ret} \qquad (1)$$
$$\boldsymbol{B}=[\boldsymbol{n}\times\boldsymbol{E}]$$

obtained from Liénard-Wiechert potentials would be used for all particles[21]. Here, $\boldsymbol{n}$ is the unit radial vector from the moving charge q to the observation point, and the usual relativistic variables β and γ are

$$\beta=\frac{v}{c} \qquad (2)$$
$$\gamma=[1-\beta^2]^{-1/2}$$

with the relativistic momentum and kinetic energy given by:

$$\boldsymbol{p}=m_o\boldsymbol{v}\gamma \qquad (3)$$
$$E=m_oc^2(\gamma-1).$$

The fields produce four main effects: magnetic fields, acceleration (radiation) fields, time retardation, and contraction of the projectile's fields in the direction of motion. Previous classical calculations using the fields above have been made by Hofstetter *et al.*[22], assuming straight-line projectile motion and a fixed target nucleus. In a latter paper these authors performed complete relativistic calculations, however, only total cross sections were reported due to high computational expense[23]. Tuebner *et al.*[24] have also used CTMC methods to calculate U^{92+} + U^{91+} cross sections. The electron in the U^{91+} case was considered to be relativistic. To simplify these calculations, the projectile motion was considered to be a straight line.

In the present work, only the field contraction is considered, while the other effects are assumed to have negligible effects on the system. It is also assumed that only the projectile will travel at relativistic velocities, since the electrons are initially non relativistic, with speed on the order of 1 a.u. In addition, low energy electron emission will be shown to make up the large majority of the ionization cross section, whereas only a very small portion, if any, of the ejected electrons will attain relativistic speeds. This assumption would not be valid if targets with higher

atomic numbers are used, where the atomic electrons will have relativistic velocities, such as the case considered by Teubner *et al.*

To justify neglecting the magnetic field on the ionization products produced by the projectile, consider that the force from the magnetic field due to the relativistic projectile is given by:

$$\boldsymbol{F} = \frac{q}{c}\boldsymbol{v}\times\boldsymbol{B}. \tag{4}$$

The magnetic field will have nearly the same magnitude as the electric field, but the force will be small due to the comparably slow particles in the target. The ratio of the magnetic to electric force is, for **E** normal to **B**, $v_{electron}/c \sim 0.01$. Moreover, the calculations by Hofstetter *et al.* did not reveal any effect on the ionized electron spectra due to the inclusion of the magnetic fields.

If the projectile is treated as an infinite mass, with constant velocity, the acceleration term must be zero. However, to obtain complete momentum balance information, the projectile must be allowed to scatter from the target. Because the uranium projectile under consideration is much heavier than the helium target and has very large momentum, the incoming ion will experience very little acceleration. For this reason, the radiation term can be ignored, but very small projectile momentum changes will be allowed.

Time retardation has also been neglected, since the impacting projectile will interact with the target from all points along its trajectory, and because the target imposes a nearly static field on the projectile. This simplification is reasonable when only the bare projectile is considered to be moving at a relativistic velocity.

After the above arguments are considered, the electric field due to the projectile is given by:

$$\boldsymbol{E} = \frac{q\boldsymbol{r}}{r^3\gamma^2(1-\beta^2\sin^2\psi)^{3/2}}, \tag{5}$$

where ψ is the angle between the projectile velocity and the radial vector to a target electron and nucleus. The field will be contracted in the longitudinal direction, and the magnitude of the

transverse field will become large with increasing projectile velocity (compared to non-relativistic impact). This field contraction will significantly decrease the collision time and the long range interaction with the projectile.

To illustrate the relativistic correction given by Eq. (5), the coulomb and relativistic longitudinal and transverse forces on a stationary electron are given in Fig. 1 for a collision by a U^{92+} projectile at a impact parameter of 2 a_o. In the transverse direction, the peak force increases linearly with γ for the 1 GeV/u impact. The integral of the transverse force is identical to that of the coulomb potential, hence, the relativistic force is much sharper and closer to the equivalent photon picture of Weizsäcker-Williams. Interestingly, the longitudinal force (whose integral is zero), decreases as γ^{-2} at large separations, giving rise to a significantly reduced post-collision interaction of the ionized target with the projectile.

Results

The collision calculations focused on single and double ionization of He by 1 GeV/u U^{92+} impact. Emphasis for single ionization is placed on the collision dynamics and the comparison of the results of including, or not including, the relativistic electric field of the projectile given by Eq. (5). For double ionization, further comparisons are made on the effects of incorporating the $1/r_{12}$ electron-electron interaction in the post-collision regime. This latter interaction is turned on after the energy of the first electron is positive relative to the target nucleus so that both the nuclear-electron and electron-electron interactions can influence the removal of the second electron. Of course, for U^{92+} impact with a q/v of 0.78, the collision is not in the perturbation regime and the nuclear-electron interaction will dominate the removal of both electrons. The $1/r_{12}$ electron-electron interaction will, however, have profound effects on the double ionization electron spectra as will be displayed later on in the text.

In Fig. 2 the longitudinal momentum spectra are shown. As can be seen from the top two theoretical figures, the change in momentum of the projectile is negligible compared to that of the electron and recoil ion. Hence, the projectile deposits the energy necessary to ionize the target, but does not appreciably participate in the momentum sharing between the electron and recoil ion as in the case of a fast, atto-second electromagnetic pulse. The two theoretical calculations were made at the same collision speed. In the top figure, non-relativistic coulomb potentials were employed. Here, we see that the electrons have a decided shift to the forward direction, and the recoils backward, due to the long-range post-collision coulomb interaction with the projectile. However, as displayed in Fig. 1, the inclusion of the relativistic projectile potential reduces the long-range longitudinal force by γ^{-2}, negating the strong post-collision interaction of the ionized products with the projectile. This results in the electrons and recoil having almost identical spectra and a decreased width for the change in the momentum of the projectile, center Fig. 2. In both cases the width of the theoretical curves for the electrons reflects the initial state Compton profile of the He atom.

Experimental values, bottom Fig. 2, nicely reflect the lack of the post-collision interaction with the projectile so that the electron and recoil ion have nearly identical longitudinal momentum spectra. However, the experimental results have a narrower half-width than the

rCTMC values. One possibility for this discrepancy is that the experimental spectra were restricted to electrons whose transverse momenta were less than 2.5 a.u., and longitudinal momenta greater than -1.92 a.u. A more probable cause is that CTMC calculations are known to suppress the soft, slow electrons produced in the collision. This deficiency is further reflected in that the CTMC absolute values are approximately a factor of four below experiment, which in turn must be tempered by the fact that the experiment was normalized to extrapolated values of Berg *et al.*[25] that have an expected precision of around a factor of two.

The calculated electron spectra differential in energy are given in Fig. 3 for the single and double ionization reactions. Also shown is the ratio of the double to single ionization cross sections in order to see its dependence on electron ejection energy. The overall general energy dependence of the cross sections for single and double ionization may be understood in terms of the relation between electron energy and impact parameter. That is fast electrons generally originate in hard, small impact parameter collisions, whereas slow electrons mainly arise from soft, large impact parameter collisions. Therefore, for low electron energies the cross section associated with the singly-charged recoil ion is expected to dominate since the double ionization probability is relatively small. On the other hand, at high electron energies double ionization dominates and the cross section associated with the higher recoil charge is larger. Such behavior is displayed in the calculated cross sections given here. This difference in the energy dependence is further illustrated by plotting the ratio of the double to single ionization cross sections. Here, we find that the ratio rises from ~1.5% for 1 eV electrons, to ~35% for 1 keV ejected electrons, reflecting the increase in double ionization transition probability relative to that for single ionization as the impact parameter is decreased.

Single ionization electron spectra differential in angle are given in Fig. 4; here, both the relativistic and non-relativistic calculations are displayed. For the two sets of calculations, there is a small, but discernable, shift for the electrons to become more centrally peaked around 90° for the relativistic case. As for the longitudinal spectra, Fig. 2, this shift is caused by the decreased post-collision longitudinal force on the ejected electron with the projectile. Within statistics, the width of the peak is effectively unchanged by including the relativistic potentials. This is probably due to the fact that the transverse force integrates to the same value for both types of

calculations, as seen in Fig. 1.

A merit of CTMC calculations is that it is possible to determine the complete kinematic balance for the single ionization products. This allows detailed insight into the 3-body collision dynamics. In Fig. 5 the momentum spectra are presented for the recoil ion, projectile, and ionized electron in the collision plane determined by the incident projectile momentum, +z-axis, and the transverse momentum of the recoil ion, +x-axis. For the system under study, the momenta of the recoil ion and the ionized electron almost balance one another. However, even in such a fast collision as this, the projectile does influence the transverse momentum balance. It is significant that there is an appreciable electron momentum component found in the same transverse direction as that of the recoil. This can only occur if the recoil ion and electron momenta are balanced by that of the projectile. Such an effect can occur in a small impact parameter collision where the projectile passes between the target nucleus and most of the electron cloud. The target nucleus is then repelled by the projectile in a transverse direction which is the same as that of the electron which experiences an attraction toward the projectile at the distance of closest approach. We find that the electron momentum spectra is also somewhat more diffuse than that of the recoil ion, further reflecting the importance of the projectile in the complete momentum balance.

Further insight into the collision dynamics can be obtained from an investigation of the azimuthal dependence of the single ionization products. A convenient representation is to plot the azimuthal angle between recoil ion and ionized electron versus that of the recoil-ion and projectile, Fig. 6. In such a representation, counts along the diagonal correspond to binary electron production with the projectile and ionized electron scattered at an azimuthal angle of 180° to one another. Significant counts along the top horizontal section correspond to strong two-body nuclear scattering where the projectile and recoil are at 180° to one another. This situation occurs in slow, molecular collisions and in fast, hard collisions when the impact parameter is small and there is an almost head-on collision between projectile and target nucleus. Counts in the right hand vertical region correspond to a dipole-like post-collision situation where the recoil ion and ionized electron are at 180° to one another. Here, the projectile deposits its energy, but does not significantly participate in the momentum sharing. Obviously, from the

previous plots, this latter situation dominates. However, there are also a significant number of counts in the upper left-hand section of Fig. 6. These are hard collisions where the projectile passes close to the target nucleus and inside most of the electron cloud of the target atom. In this situation there is strong 180° repulsive scattering between the heavy particles, with the electron being attracted toward the projectile in the same direction as the recoil. This is also the same reason for both the recoil and electron being observed in the same positive collision plane of Fig. 5.

The correlation between the ionized electron and recoil ion can be further illuminated by plotting the differential cross section in terms of the azimuthal angle between the two. Such a plot is given in Fig. 7. Clearly, there is a strong correlation between the recoil ion and ionized electron with a full width-half maximum spread of only ~25° centered around 180°. Thus, this collision system very closely portrays the Weizsäcker and Williams equivalent photon hypothesis.

Although the experimental detection of both electrons and the recoil ion in the double ionization reaction suffered substantially from low count rates, it is instructive to extend the calculations to this reaction. Further, since it is possible to include, or not include, the $1/r_{12}$ electron-electron interaction after the first electron's energy becomes positive relative to the target nucleus, the effects of electron correlation in the post-collision regime can be explored in detail.

A convenient method to illustrate the outgoing electron correlation is to plot the longitudinal momentum of one electron relative to that of the other, Fig. 8. In this manner, the diagonal pointing into the first quadrant represents the sum momenta given to the electrons, while the diagonal pointing to both the second and fourth quadrants yields the difference in the momenta of the two electrons. As can be seen in the lower figure, no correlation between electrons is realized if the $1/r_{12}$ interaction is not included. Such is what one would expect from independent electrons. Moreover, the plot is centrally distributed, illustrating that the post-collision interaction with the projectile is again negligible as in the single ionization case. The inclusion of the $1/r_{12}$ interaction dramatically changes the distribution, top figure. Now the sum momenta is still located at zero as in the independent electron case, however, the distribution is

considerably broadened along the difference momenta diagonal, and is rectangular, not circular, in shape. The rectanglar distribution implies that the inclusion of the $1/r_{12}$ interaction causes the two electrons to no longer equally share the longitudinal momenta, but to distribute it such that if one electron is fast, the other will be slow, and vice versa. Previously, we have demonstrated a similar behavior for kinematically complete double ionization measurements and calculations[4] for 3.6 MeV/u Se^{28+}. The rectanglar distribution of the top figure is also consistent with the equivalent photon calculations of Keller *et al.*[20]. Their results show that the $1/r_{12}$ post-collision interaction for $b = 5\ a_o$ will give a shape similar to that presented here. Moreover, they predict that initial state angular correlation, which we do not include in our model, will further modify the longitudinal momentum pattern to become almost star shaped with lobes pointing along the axes. This situation occurs if the collision is sufficiently fast, and the charge state of the projectile is low enough for application of the perturbation method.

The electron-electron correlation can be further shown by plotting the azimuthal angular dependence between the two outgoing electrons. As expected, the lack of the $1/r_{12}$ electron-electron interaction results in a distribution that is almost isotropic. There is a tendency for this cross section to be peaked near 0^o since the sum momenta of the two electrons must balance that of the recoil ion, and are both born in independent collisions that pull both electrons toward the projectile at the distance of closest approach. Inclusion of the post-collisional $1/r_{12}$ interaction changes the picture completely, and nicely demonstrates the tendency for both electrons to be emitted in opposite azimuthal angles to one another.

Conclusions

In this paper, we have presented the first kinematically complete calculations for single and double ionization of He in relativistic collisions. The longitudinal momentum spectra of the ionized electron and recoil ion show the effects of the Lorentz contraction of the electric field provided by the projectile, with the concomitant reduction of the post-collision interaction of the electron and recoil ion by the out-going projectile. Collision plane studies provide information that the projectile's momentum is only changed slightly during the collision, so that the recoil ion and electron are emitted almost back-to-back. This observation lends credibility to the use of an equivalent photon approach to explain these collisions, a method proposed well in the past by Weizsäcker and Williams[18,19].

The inclusion of the $1/r_{12}$ electron-electron interaction in the rCTMC calculations for double ionization displayed clear effects on the outgoing electrons. Here, the longitudinal momentum distributions showed the tendency for an unequal sharing of momenta so that if one electron is fast, the other is slow, and vice versa. Likewise, there is a significant angular correlation of the ionized electrons even when the $1/r_{12}$ interaction is only included in the post-collisional regime. These effects were further emphasized by completing identical calculations where the $1/r_{12}$ interaction was not incorporated.

Future experiments will aim to perform complete kinematic measurements for double ionization in the perturbation region where the expected experimental count rate is low. This will require considerable modification of our experiment, but is feasible, and will allow us to directly observe electron-electron correlation in the limit of fast collisions with light projectiles.

Acknowledgments

The authors would like to acknowledge the support from the Office of Fusion Energy of DOE (REO and CJW), from the Gesellschaft für Schwerionenforschung (CJW, RM and JU), and from the Deutsche Forschungsgemeinschaft (RM).

References

1. J. Ullrich, R. Moshammer, R. Dörner, O. Jagutzki, V. Mergel, H. Schmidt-Böcking and L. Spielberger, *J. Phys. B* (accepted) (1997).

2. C. L. Cocke and R. E. Olson, *Phys. Reports* **205**, 155 (1991).

3. R. Moshammer, J. Ullrich, M. Unverzagt, W. Schmitt, P. Jardin, R. E. Olson, R. Dörner, V. Mergel and H. Schmidt Böcking, *Phys. Rev. Lett.* **73**, 3371 (1994).

4. R. Moshammer, J. Ullrich, H. Kollmus, W. Schmitt, M. Unverzagt, O. Jagutzki, V. Mergel, H. Schmidt Böcking, R. Mann, C. J. Wood and R. E. Olson, *Phys. Rev. Lett.* **77**, 1242 (1996).

5. R. Moshammer, J. Ullrich, H. Kollmus, W. Schmitt, M. Unverzagt, H. Schmidt Böcking, C. J. Wood and R. E. Olson, *Phys. Rev. A* (accepted) (1997).

6. R. Abrines and I. C. Percival, *Proc. Phys. Soc. Lond.* **88**, 873 (1966).

7. R. E. Olson and A. Salop, *Phys. Rev. A* **16**, 531 (1977).

8. R. E. Olson, J. Ullrich and H. Schmidt-Böcking, *Phys. Rev. A* 39, 5572 (1989).

9. M. Unverzagt, R. Moshammer, W. Schmitt, R. E. Olson, P. Jardin, V. Mergel, J. Ullrich and H. Schmidt-Böcking, *Phys. Rev. Lett.* **76**, 1043 (1996).

10. V. J. Montemayor and G. Schiwietz, *Phys. Rev. A* **30**, 30 (1984).

11. L. Meng, R. E. Olson, R. Dörner, J. Ullrich, and H. Schmidt Böcking, *J. Phys. B* **26**, 338 (1993).

12. V. Mergel et al. *Phys. Rev. Lett.* (accepted) (1997).

13. V. Frohne, S. Cheng, R. M. Ali, M. L. Raphaelian, C. L. Cocke, and R. E. Olson, *Phys. Rev. A* **53**, 2407 (1996).

14. C. J. Wood and R. E. Olson, *J. Phys. B* **29**, L257 (1996).

15. R. E. Olson, C. R. Feeler, C. J. Wood, C. L. Cocke, R. Dörner, V. Mergel, H. Schmidt-Böcking, R. Moshammer and J. Ullrich, *Nucl. Instr. and Meth. B* **124**, 249 (1997).

16. R. E. Olson, J. Wang, and J. Ullrich, *XVIIIth The Physics of Electronic and Atomic Collisions - Invited Papers*, ed. by T. Andersen, B. Fastrup, F. Folkmann, H. Knudsen, and N. Andesrsen (AIP Conf. Proc. 295, New York, 1993) pp. 520-33.

17. J. Eichler and W. E. Meyerhof, *Relativistic Atomic Collisions* (Academic Press, San Diego 1995).

18. C. F. Weizsäcker, *Z. Phys.* **88**, 612 (1934).

19. E. J. Williams, *Phys. Rev.* **45**, 729 (1934).

20. S. Keller, H. J. Lüdde and R. M. Dreizler, *Phys. Rev. A* (accepted) (1997).

21. J. D. Jackson, *Classical Electrodynamics* (Wiley, New York, 1975) pp 552-6.

22. S. Hofstetter, C. Hofmann, and G. Soff, *Z. Phys. D* **23**, 227 (1992).

23. S. Hofstetter, N. Grün, and W. Scheid, *Z. Phys. D* **37**, 1 (1996).

24. E. Teubner, G Terlecki, N Grün, and W. Scheid, *J. Phys. B* **13**, 523 (1980).

25. H. Berg, J. Ullrich, E. Bernstein, M. Unverzagt, L. Spielberger, J. Euler, D. Schardt, O. Jagutzki, H. Schmidt-Böcking, R. Mann, P. H. Molker, S. Hagmann, and R. D. Fainstein, *J. Phys. B* **25**, 3655 (1992).

Figure Captions

1. Relativistic transverse and longitudinal forces on an electron test particle at the origin induced by a U^{92+} projectile at an impact parameter of $b = 2\ a_o$, and a speed of $\beta = 0.88$ ($\gamma = 2.1$).

2. Longitudinal momentum spectra for the electron and recoil ion, and the change in momentum for the projectile in 1 GeV/u U^{92+} + He single ionization collisions. Top figure: non-relativistic calculation for $\beta = 0.88$, center figure: inclusion of the relativistic potential for the projectile, and bottom figure: experimental data.

3. Calculated electron spectra differential in the energy of the ejected electron for single and double ionization. In the lower figure, the ratio of double to single ionization is presented as a function of ejected electron energy.

4. Calculated relativistic (open circles) and non-relativistic (line), cross sections for the single ionization electron spectra differential in the angle of the ejected electron.

5. Three-body momentum spectra for the recoil ion, ionized electron, and projectile momentum change, are given in terms of the collision plane defined by the incident projectile momentum, and the transverse momentum of the outgoing recoil ion. The plots were made using a linear scale where each contour line represents equal portion of the total cross section.

6. Correlation in the azimuthal angle between the recoil ion that of the ionized electron and projectile. A logarithmic scale was used with eight contour lines being distributed between 20 and 1,000 counts in each 4° x 4° bin.

7. Azimuthal angle differential cross section between the ionized electron and the recoil ion for single ionization.

8. Calculated correlation in the longitudinal momentum dependence of the two outgoing electrons for 1 GeV/u U^{92+} + He double ionization collisions. The top and lower figures compare the results of performing the calculations with, and without, the inclusion of the electron-electron $1/r_{12}$ interaction in the post-collision regime. The plots were made using a linear scale where each contour line represents equal portion of the total cross section.

9. Calculated correlation in the azimuthal momentum dependence of the two outgoing electrons in double ionization. The solid and open circles compare the results of performing the calculations with, and without, the inclusion of the electron-electron $1/r_{12}$ interaction in the post-collision regime.

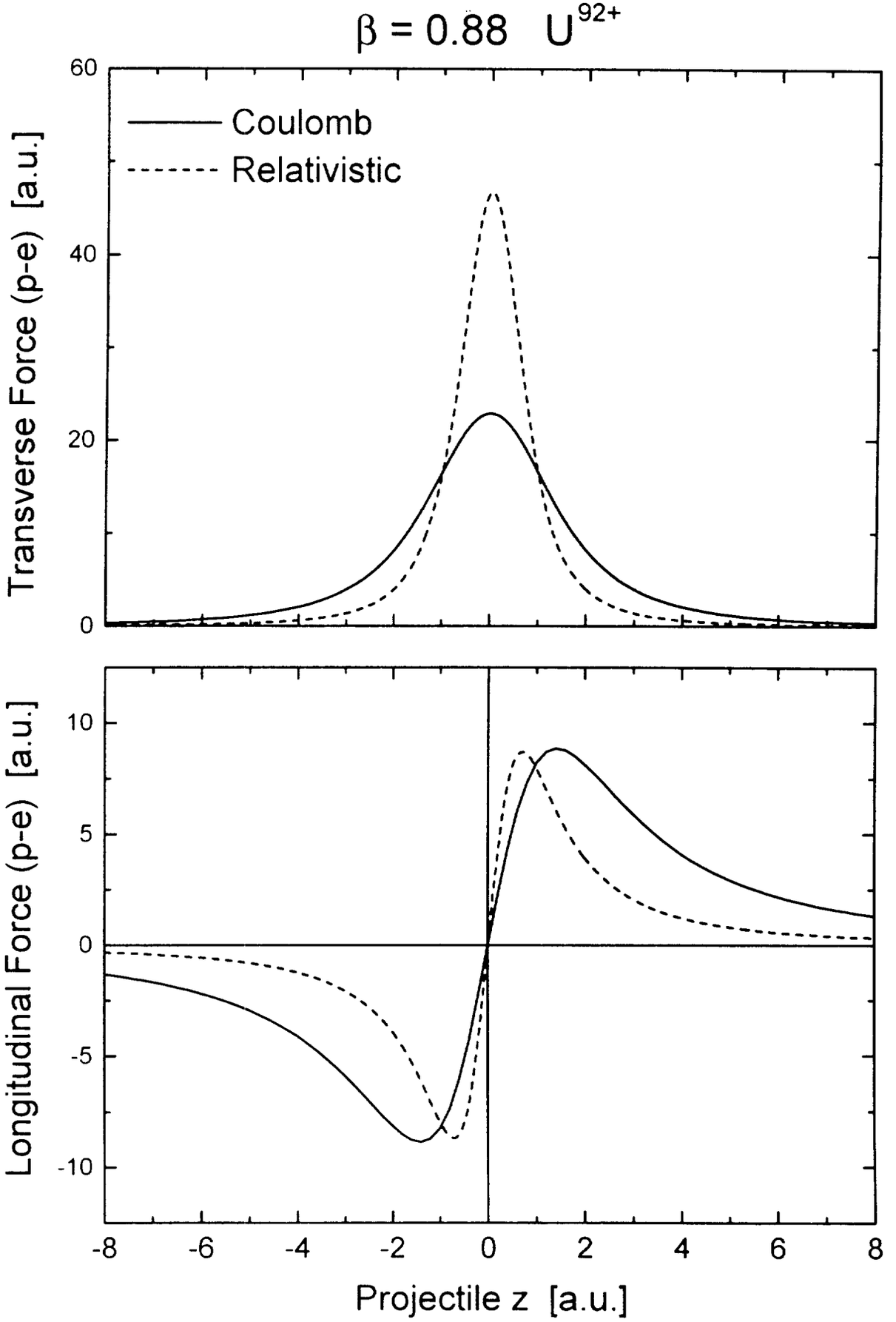

Fig. 1

Fig. 1 Ullrich et al PRA

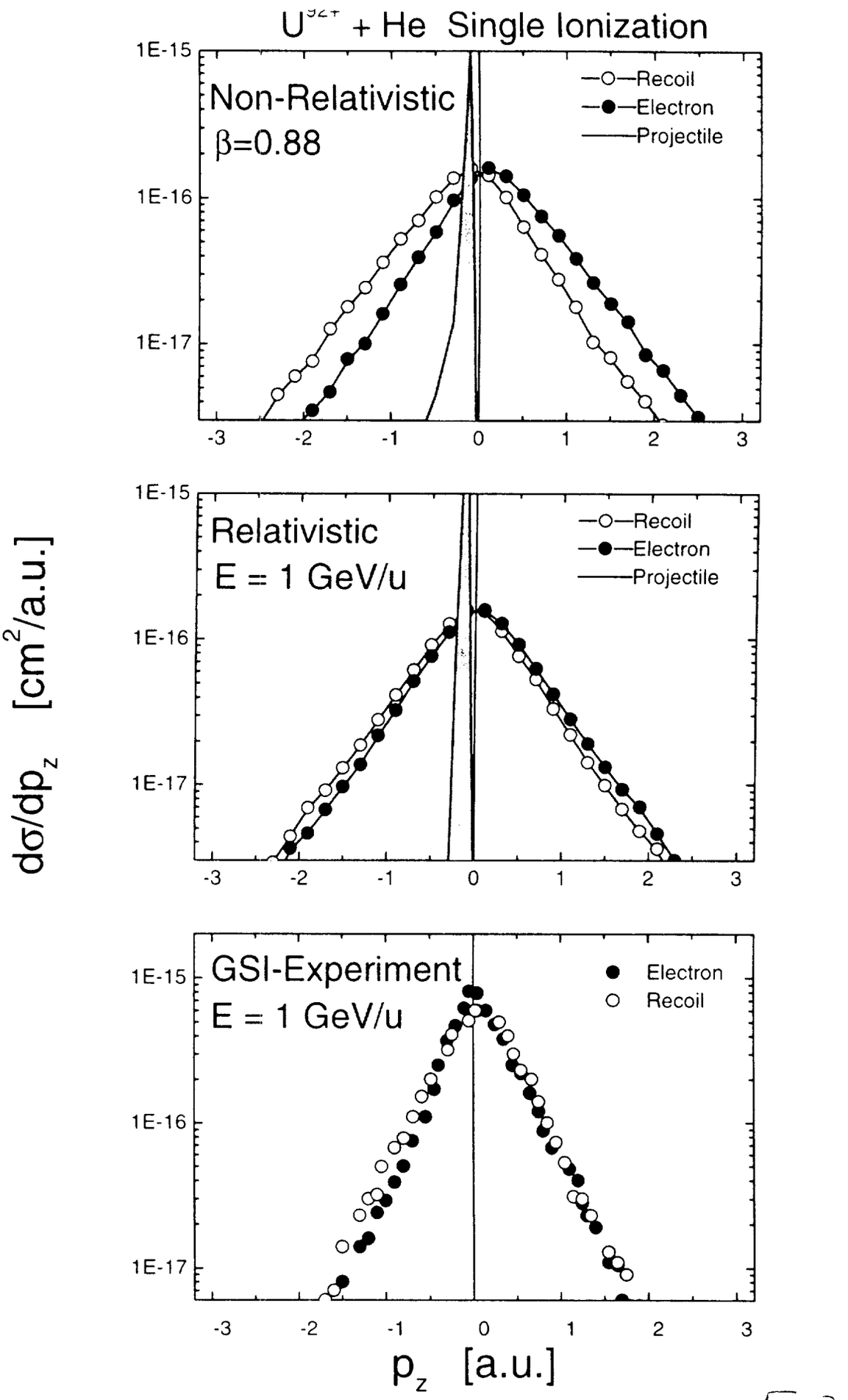
U92+ + He Single Ionization
Non-Relativistic
β=0.88
Recoil
Electron
Projectile
Relativistic
E = 1 GeV/u
GSI-Experiment
E = 1 GeV/u
dσ/dp_z [cm²/a.u.]
p_z [a.u.]
1E-15
1E-16
1E-17
-3
-2
-1
0
1
2
3

Fig 2

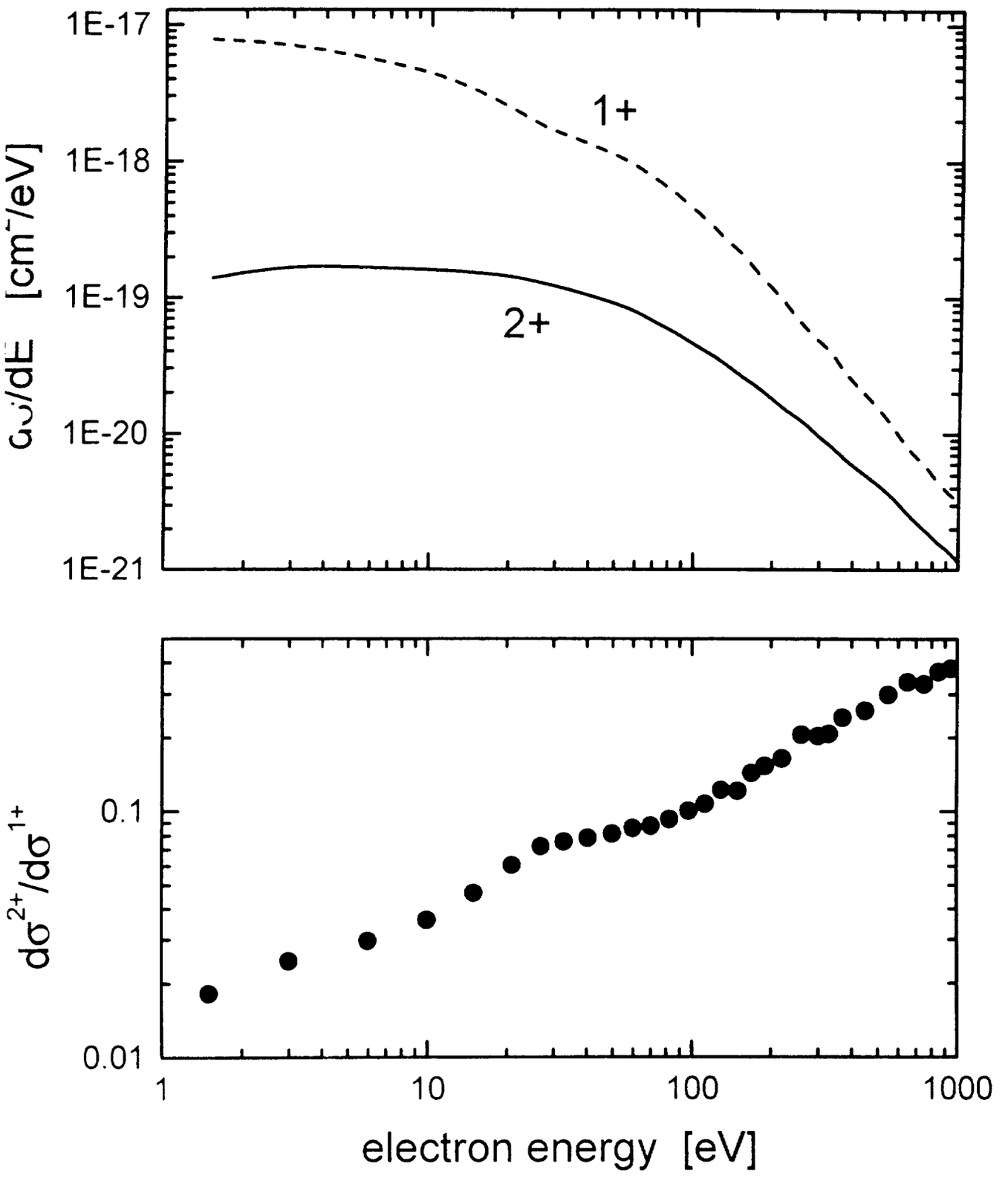
U92+ + He 1 GeV/u
1E-17
1E-18
1E-19
1E-20
1E-21
1+
2+
dσ/dE [cm²/eV]
0.1
0.01
dσ2+/dσ1+
1
10
100
1000
electron energy [eV]

Fig 3

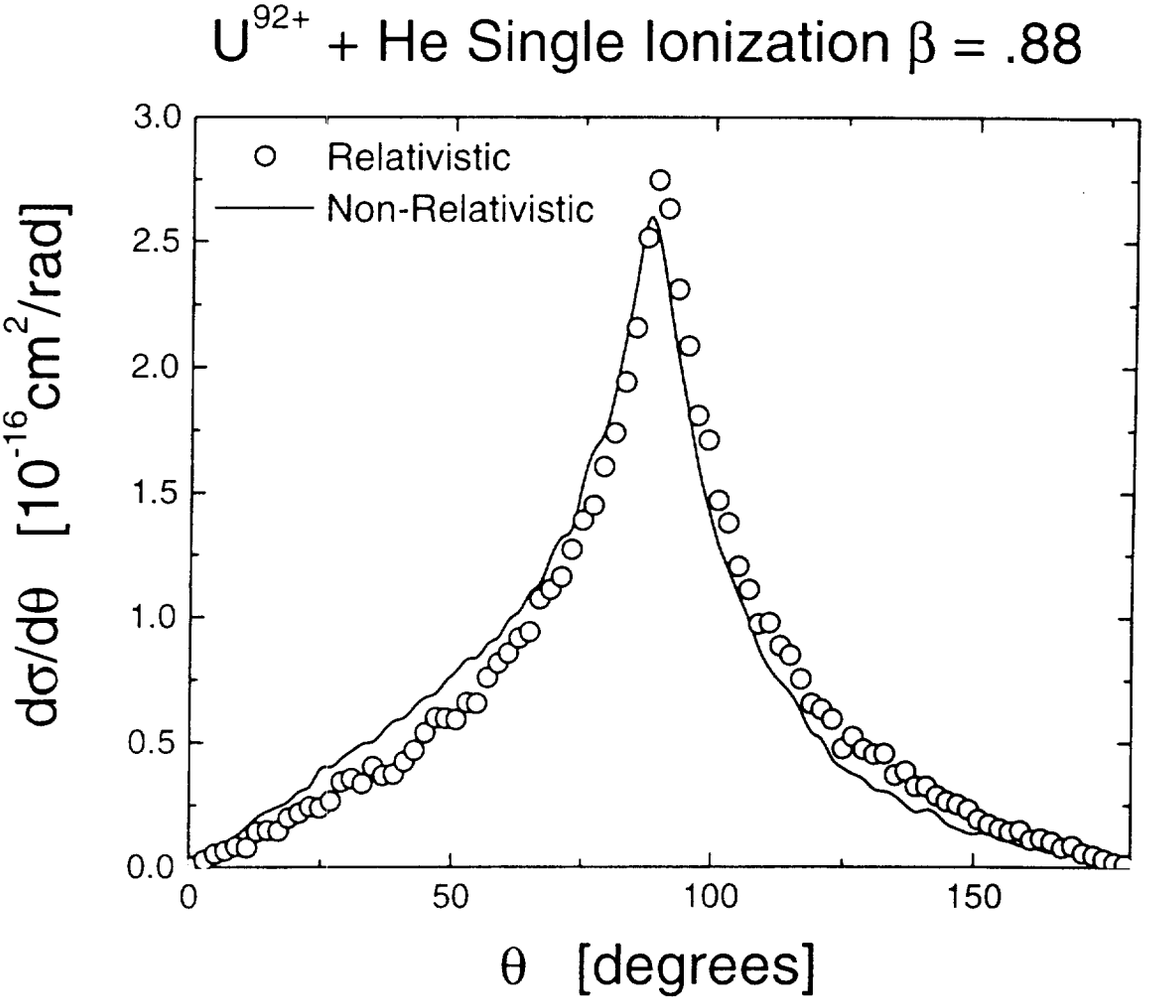

Fig. 4

Fig. 4 Wood et al. PRA

U^{92+} + He Single Ionization β=0.88

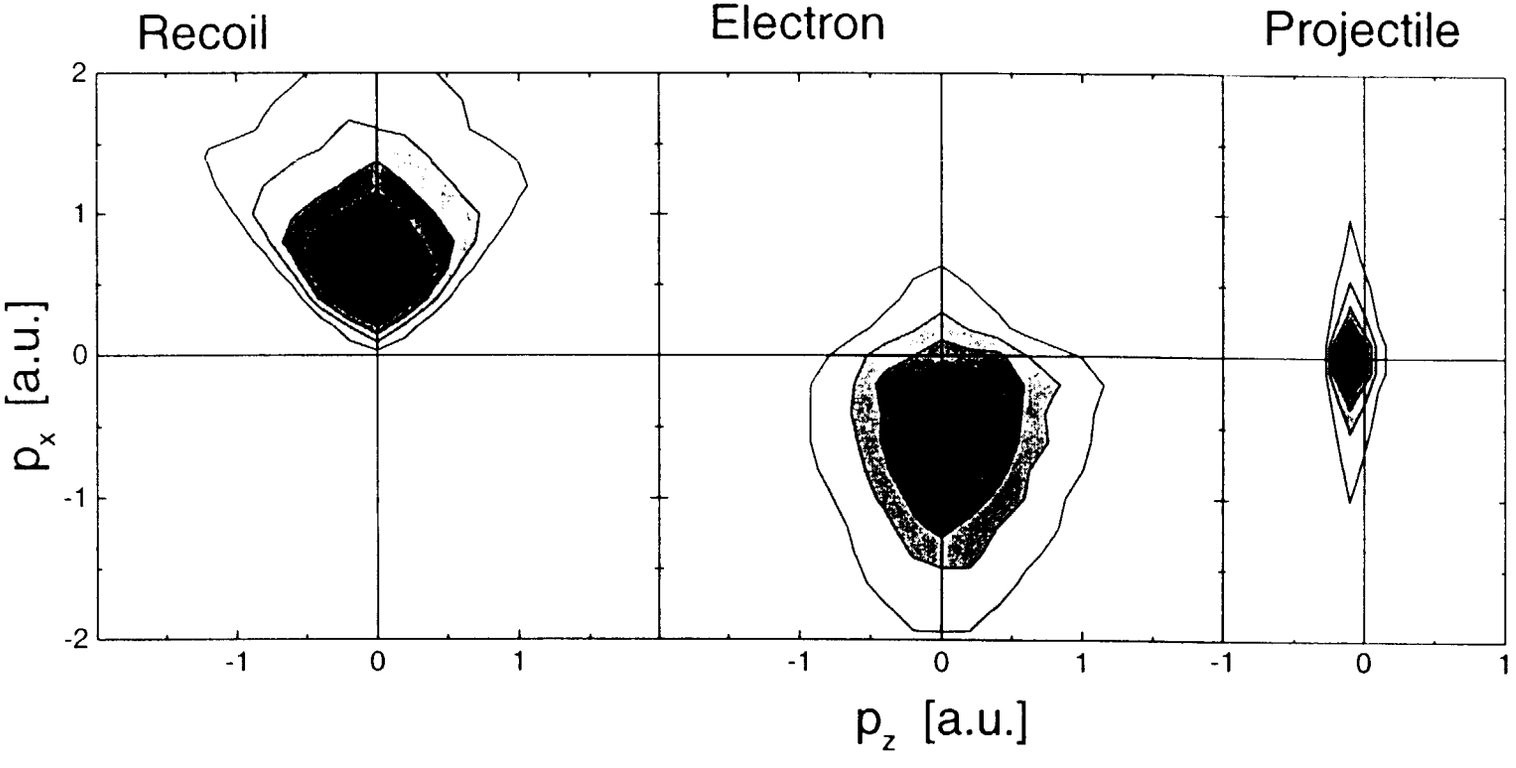

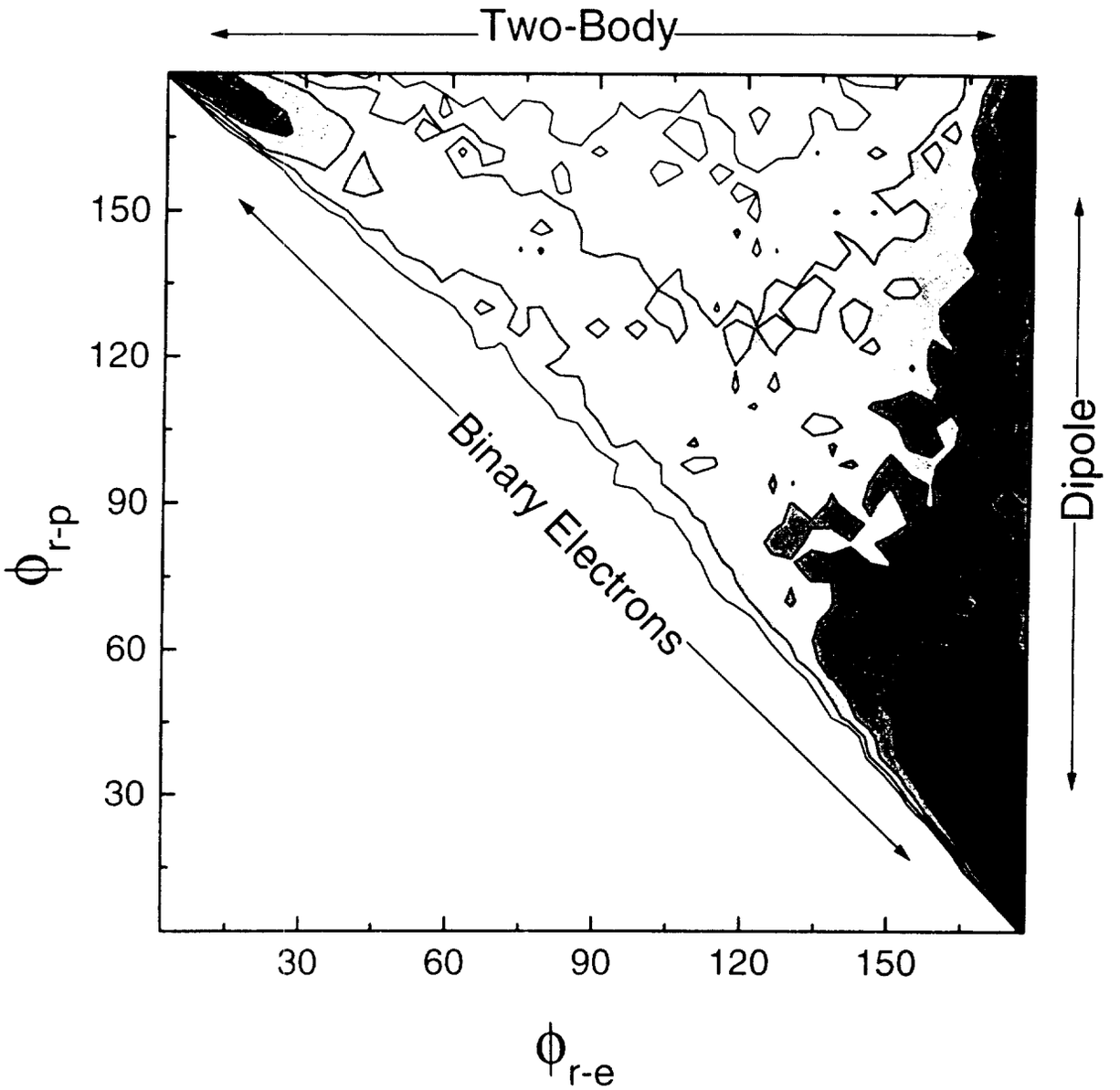
Two-Body
Dipole
Binary Electrons
150
120
90
60
30
$\phi_{r\text{-}p}$
30
60
90
120
150
$\phi_{r\text{-}e}$

Fig 6

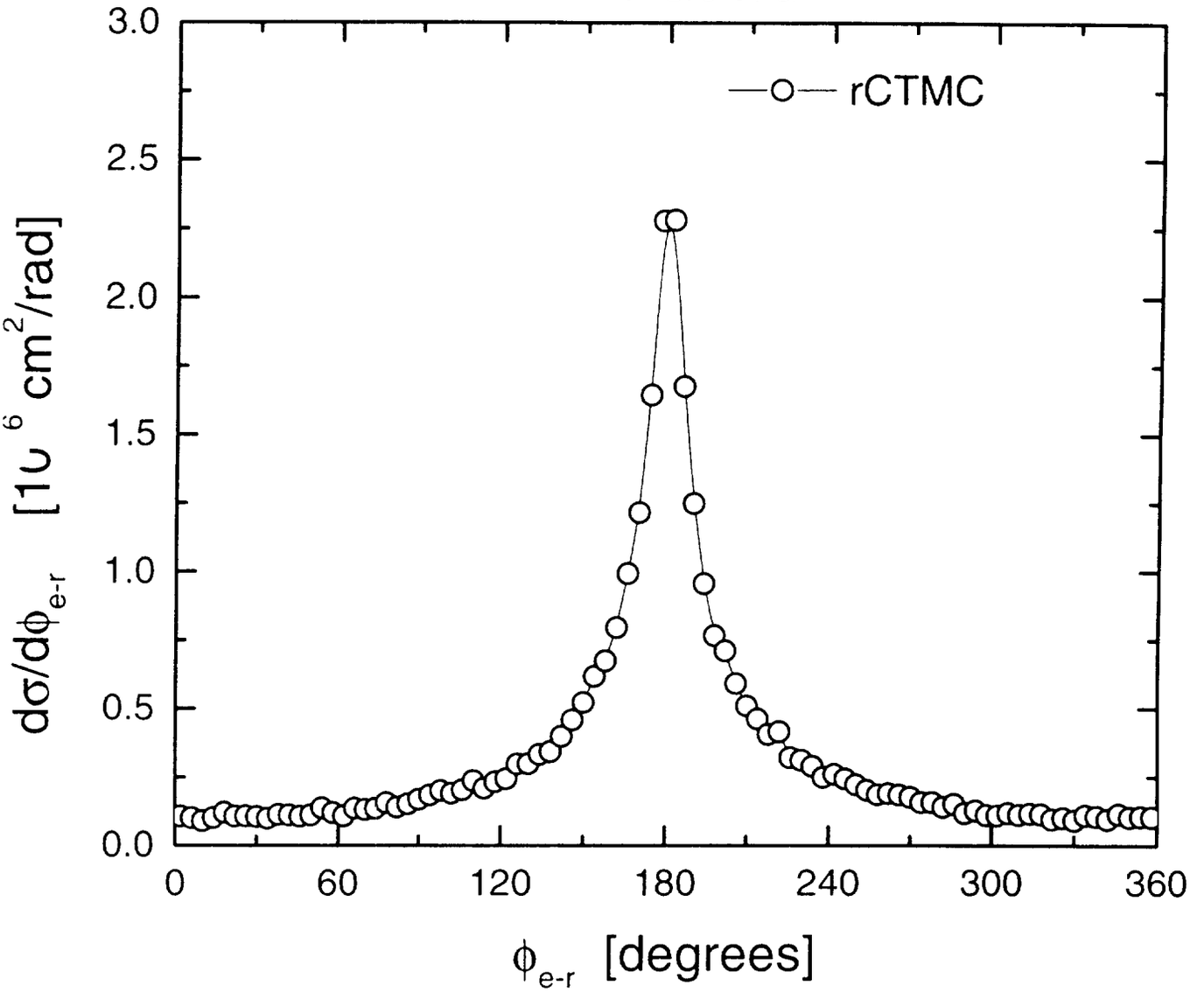

Fig 7

Fig 7 Ward et al. PRA

U^{92+} + He Double Ionization 1 GeV/u

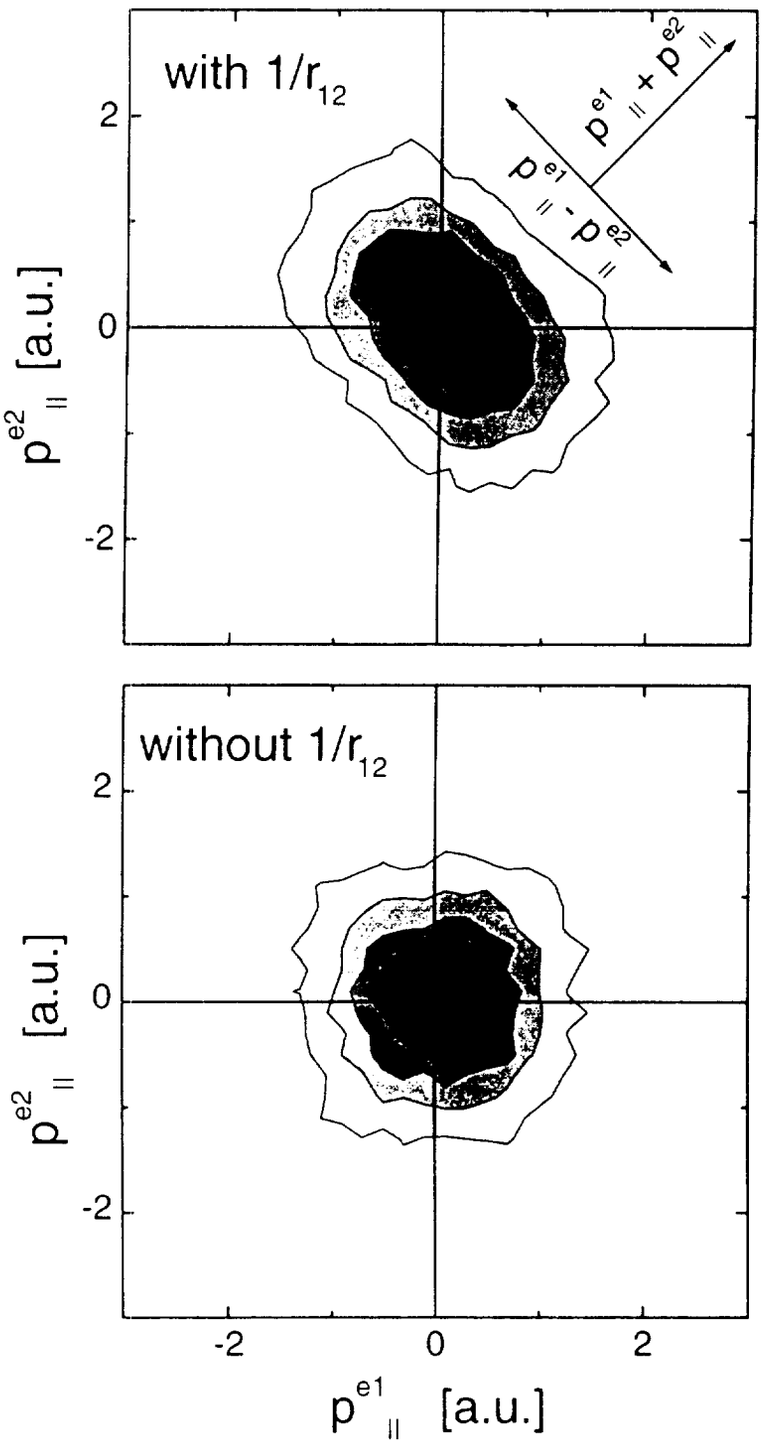

Fig. 3

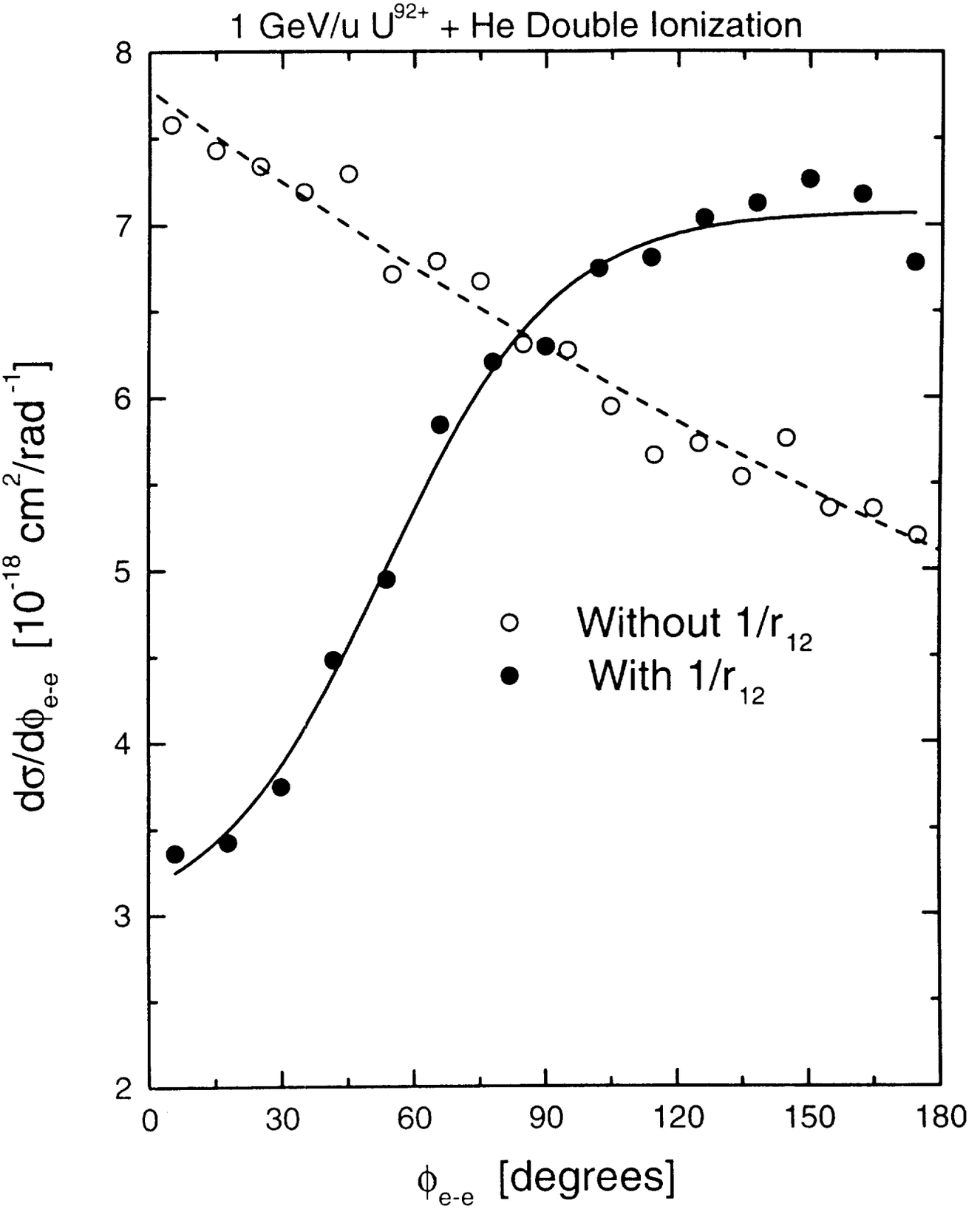

Fig 9

Fig 9 Wood et al PRA